Chaos, Solitons and Fractals 144 (2021) 110620

Contents lists available at ScienceDirect

Chaos, Solitons and Fractals

Nonlinear Science, and Nonequilibrium and Complex Phenomena

journal homepage: www.elsevier.com/locate/chaos

Deterministic and stochastic analysis for different types of regulations in the spontaneous emergence of cell polarity

Yue Liu*, Wing-Cheong Lo

Department of Mathematics, City University of Hong Kong, Tat Chee Avenue, Kowloon, Hong Kong, China

ARTICLE INFO

Article history:
Received 15 July 2020
Revised 20 November 2020
Accepted 21 December 2020

Keywords:
Reaction-diffusion system
Non-local kinetics
Stochastic model
Linear noise approximation
Feedback regulation

ABSTRACT

Spontaneous emergence of cell polarity intrinsically lies at the localization of signaling molecules on a particular region of cell membrane. Such a process necessarily contains a positive feedback loop to amplify the localized cluster. To describe the polarizing process and explore different feedback functions involved, deterministic and stochastic models with non-local kinetics are discussed in this paper. Stochastic Simulation Algorithm (SSA) is used to numerically simulate the polarizing behavior and analytical analysis by the power spectrum is applied to approximate the parameter regime for the spontaneous emergence of cell polarity. Compared to the results from the deterministic model, we can understand how the stochastic effect extends the parameter regime for achieving cell polarization under different types of feedback, including the forms of quadratic function, linear function, and Hill function. Both deterministic and stochastic methods fail to yield the polarity at a low number of molecules. Our results suggest that the parameter region for cell polarization under the Hill function feedback is smaller than that with the quadratic function feedback.

1. Introduction

Cell polarity is a crucial attribute of cellular functions for ensuing directed growth, locomotion, and differentiation. It intrinsically lies at the localization of signaling molecules on a certain region of cell membrane [1]. Budding yeast has been proved to be a powerful model system for studying the mechanism of cell polarity establishment. In a yeast cell, the budding process fundamentally depends on the signaling protein Cdc42. When a yeast cell received the indication of intracellular or extracellular cues, Cdc42, which consists of guanosine triphosphate (GTP) and guanosine diphosphate (GDP) bound forms, in the cytoplasm will be recruited to the membrane. Such recruitment involves the exchange of signaling molecules, feedbacks by molecular interactions, molecular transportation and diffusion. During the process, the positive feedback loop by local activation of Cdc42 plays a vital role in generating a cluster of concentrated Cdc42 at the cell membrane [2–4]. Moreover, a negative feedback loop has also been investigated and concluded to enhance the robustness of polarity [5,6]. Without guidance from the spatial cue, cells can spontaneously go through the polarizing process, namely symmetry breaking [7,8].

Mathematical modelings through deterministic and stochastic systems have been used to study cell polarization in many studies [2,6,9–14]. Based on deterministic reaction-diffusion equations (RDEs), Turing mechanism and wave-pinning mechanism have been applied to explain symmetry breaking of yeast polarization [2,10,14–16]. Another way to understand symmetry breaking is through stochastic modeling. Altschuler et al. [9] showed that a stochastic model with linear positive feedback is sufficient to achieve symmetry breaking. Walther et al. [17] considered discrete molecular distribution with local recruitment in the wave-pinning model and concluded that the polarizing phenomenon was lost due to stochastic fluctuations. Pablo et al. [13] applied particle-based simulations to find that molecular-level fluctuations can facilitate cell polarization. A stochastic neutral drift polarity model was proposed in [16] which predicted that below a critical density of signaling molecules, positive feedback maintained an off state robustly and, over this critical threshold, it switched on the recurrent emergence of localized clusters. These studies were mainly restricted to their own settings of feedback function but not compare the polarizing behaviors under different forms of feedback. Therefore, we are motivated to answer the following questions in this paper: What are the polarizing behaviors in deterministic and stochastic models with different forms of feedback? How does stochastic fluctuation affect the parameter regime for achieving cell polarization? Is this behavior affected by different feedback functions?

* Corresponding author.
E-mail address: yue.liu@my.cityu.edu.hk (Y. Liu).

https://doi.org/10.1016/j.chaos.2020.110620
0960-0779/

The paper is organized as follows. In Section 2, deterministic and stochastic models incorporating a general feedback form for the spontaneous emergence of cell polarity are introduced. In Section 3, we apply the linear noise approximation on the stochastic model to derive power spectrum. In Section 4.1, deterministic and stochastic behaviors of cell polarization with quadratic feedback function are illustrated. Parameter regimes predicted by Turing instability analysis, Stochastic Simulation Algorithm (SSA), and power spectrum are compared. Our results demonstrate that the parameter regime predicted by the power spectrum fits well with that obtained by SSA. In Sections 4.2 and 4.3, comparisons of parameter region obtained with feedback in the form of linear function and Hill function are discussed, respectively. And then the comparison of localization behaviors with different limitations of recruitment is given in Section 4.4. Finally, the main results are concluded in Section 5.

2. Mathematical models

2.1. The deterministic model with general feedback form

A continuum model is developed to describe the dynamics of polarized signaling molecules on the cell membrane in this section. We use a system of RDEs to model the cell polarization process. Here the main factors in this process include the membrane-bound signaling molecules in active GTP-bound and inactive GDP-bound forms ("active" form indicates that only this form is functional to induce the downstream cellular responses, although the "inactive" molecules are also important in the cycling of molecules). Besides the membrane-bound molecules, the cytoplasmic inactive form molecules are also implicitly involved through the conservation of total molecules. The change from an active form to an inactive form is initiated by hydrolysis and is reversely regulated by guanine nucleotide exchange factors (GEFs). When the signaling molecules are in an inactive form, guanine nucleotide disassociation inhibitors (GDIs) bind to the molecules and release them from the cell membrane to cytoplasm. Synthesis and degradation of signal molecules are excluded since the timescales are slower compared to the dynamics of polarization [4].

The domain in our model is the membrane surrounding a well-mixed cytoplasmic region, which is a sphere in two-dimension, or for simplicity, it could be the cross-section of the cell, which is a circle in one-dimension. Two variables, $a(x,t)$ and $b(x,t)$, are used to represent active and inactive membrane-bound signaling molecules and to avoid confusion, they also denote the corresponding particle concentrations [9]. Dynamics of a and b are thus governed by a reaction-diffusion system which is regulated by a positive feedback function $F(\cdot)$:

$$\frac{\partial a}{\partial t} = D_m\nabla^2 a + F(a)b - k_{off}a, \tag{1a}$$

$$\frac{\partial b}{\partial t} = D_m\nabla^2 b - F(a)b + k_{off}a + g_{on}(N-\widetilde{a}-\widetilde{b})Q(a,b) - g_{off}b, \tag{1b}$$

where $(N-\widetilde{a}-\widetilde{b})$ is the non-local function with $\widetilde{a}=\int a\ dS$ and $\widetilde{b}=\int b\ dS$ respectively representing the total numbers of a and b over the cell membrane. The first term on the right-hand side in (1a) and (1b) represents the diffusion of species a and b with the lateral surface diffusion rate D_m and the Laplacian operator ∇^2 on the cell membrane. Here we consider the same diffusion coefficient D_m for a and b [2,18].

In our model, the non-local kinetics of recruiting inactive molecules from the whole cytoplasm are considered and the recruiting rate is g_{on}. We assume that the total number of active and inactive signaling molecules in the whole cell is conserved to be N where synthesis and degradation are excluded. Along with the fact that $\widetilde{a}$ and $\widetilde{b}$ represent the total number of the membrane-bound species, we obtain that $(N-\widetilde{a}-\widetilde{b})$ stands for the amount of cytoplasmic inactive signaling molecules. Since the transportation of cytoplasmic molecules is relatively fast, we assume that the recruitment of inactive signaling molecules from the cytoplasm to the membrane is proportional to the amount of cytoplasmic inactive signaling molecules. To match with the definition of N, the initial value for $\widetilde{a}+\widetilde{b}$ needs to be less than N. If there is an upper limit for the particle density at a local position on cell membrane, we define the function $Q(a,b)$ as

$$Q(a,b) = 1 - \frac{a+b}{\Omega},$$

where the parameter Ω is the carrying capacity for measuring the maximum particle concentration at a local position on cell membrane; if not, i.e., $\Omega \gg (a+b)$, then we can set $Q(a,b)\equiv 1$ to remove the limit on the recruitment of inactive signaling molecules from the cytoplasm. In the last term of Eq. (1b), g_{off} is the rate at which inactive signaling molecules are extracted from the membrane into the cytoplasm and this process is facilitated by GDIs. The constant k_{off} is the deactivation rate coefficient of signaling molecules from an active form to an inactive form.

In (1a)–(1b) system, feedback regulation occurs through the function F which represents the activation rate of signaling molecules. By assuming that active signaling molecules form a feedback loop to promote activation, the function F is thus positively correlated with the particle density of a. Experimental studies [2,18,19] have suggested that two forms of positive regulations enable the active signaling molecules to localize and induce the cell polarity. One is that the activation of Cdc42-GTP is mediated by GEFs in a positive quadratic or linear feedback function form Goryachev and Pokhilko [2], Lo et al. [18]:

$$F(a) = k_{11} + k_{12}a^n, \tag{2}$$

where k_{11} represents the basal activation rate of Cdc42, k_{12} represents the activation rate from the feedback loop, and the degree of cooperativity $n=1$ or 2 corresponds to linear or quadratic feedback loop. This function form is direct cooperative feedback depending on the local density of active molecule a, which has been used in many Turing type systems [15,20]. Another case is that the activation of Cdc42-GTP can saturate and it obeys a Hill function [19]:

$$F(a) = k_{21} + k_{22}\frac{a^n}{k_{23}^n + a^n}. \tag{3}$$

where k_{21} is the activation rate, k_{22} is the magnitude of self-activation, and k_{23} represents the saturation constant. Kinetic in Hill form is a critical feature for the wave-pinning mechanism which requires the bistability [10]. This form shows a locally increasing recruitment rate at a low Cdc42-GTP density, but the rate is bounded at a high Cdc42-GTP density. Feedback regulations (2) and (3) include multi-step cooperative interactions such as recruitment and binding. These multi-step cooperations are modeled through the term a^n with $n\geq 2$. The parameters used in the model are listed in Table 1.

We apply Turing stability analysis to identify rules of choosing parameters for achieving symmetry breaking. Here the cell membrane is treated as a circle with radius $R\ \mu m$ (length of the whole membrane $L=2\pi R\ \mu m$ and $x\in[0,L]$) in a one-dimensional spatial domain, so that the curvature effects will be ignored. The details of Turing stability analysis can be found in Appendix A. Cell polarity establishment relies on the instability of the homogeneous steady state. The eigenvalues of Jacobian matrix evaluated at the homogeneous steady state yield the following two conditions for achieving cell polarity:

(i) If the perturbation is spatially homogeneous, the homogeneous steady state (a^*, b^*) is stable and the real parts of all eigenvalues of the Jacobian matrix are negative.
(ii) For the positive wavenumber k, at least one eigenvalue is positive, which means the instability of the homogeneous solution only occurs with positive wavelengths. A perturbation will grow and may lead the solution to an inhomogeneous state from the homogeneous steady state.

These two conditions imply that wave functions perturbed from the homogeneous state are moving toward another steady state for and only for positive wavelengths. If there exists the critical wavenumber k_c such that for any positive integer $k \leqslant k_c$, Turing instability holds if system (1a)–(1b) satisfies the following two conditions

$$F'b^* - k_{off} - \frac{g_{on}\frac{N-a^*L-b^*L}{\Omega} + g_{on}QL}{g_{on}\frac{N-a^*L-b^*L}{\Omega} + g_{on}QL + g_{off}}F < 0, \tag{4}$$

and

$$-\sigma_1 D_m + F'b^* - k_{off} - \frac{\sigma_m D_m + g_{on}\frac{N-a^*L-b^*L}{\Omega}}{\sigma_m D_m + g_{on}\frac{N-a^*L-b^*L}{\Omega} + g_{off}}F > 0. \tag{5}$$

2.2. The stochastic model and the master equation

For simplicity, we consider the cell membrane as a one-dimensional domain with length L and the domain is partitioned into K identical compartments with uniform length h, where $h = L/K$. The subsystem in each compartment is assumed to be homogeneous. Same types of molecules in different compartments are treated as different species, denoted by $\{A_1, \ldots, A_k, \ldots, A_K, B_1, \ldots, B_k, \ldots, B_K\}$, where A_k and B_k are the active and inactive membrane-bound signaling molecules in the kth compartment, respectively. In this section, index k will be used to indicate the kth compartment. The system state is denoted by $\mathbf{X}(t) = (\vec{X}, \vec{Y}) = (x_1(t), \ldots, x_k(t), \ldots, x_K(t), y_1(t) \ldots, y_k(t) \ldots, y_K(t))$, where $x_k(t)$ and $y_k(t)$ are the numbers of active and inactive membrane-bound signaling molecules in the kth compartment, respectively.

Only molecules in the same compartment can react. Thus in each well-mixed compartment, there are four types of reactions: activation, deactivation, recruitment, and dissociation. We have the following

$$R_{k1} : B_k \xrightarrow{\gamma_{k1}} A_k, \quad R_{k2} : A_k \xrightarrow{\gamma_{k2}} B_k,$$
$$R_{k3} : \emptyset \xrightarrow{\gamma_{k3}} B_k, \quad R_{k4} : B_k \xrightarrow{\gamma_{k4}} \emptyset,$$

where $\emptyset$ represents chemical species which are not further involved in following process; γ_{kj} $(j = 1, 2, 3, 4)$ is the reaction rate constant of reaction R_{kj} in the kth compartment. R_{k1} is the activation process and $\gamma_{k1} = F(x_k/h)$; R_{k2} is the deactivation process and $\gamma_{k2} = k_{off}$; R_{k3} is the recruitment process and $\gamma_{k3} = g_{on}(N - \sum_k (x_k + y_k))Q(x_k/h, y_k/h)$; R_{k4} is the dissociation process and $\gamma_{k4} = g_{off}$. The *propensity functions* α_{kj} for reactions are defined as:

$$R_{k1} : \alpha_{k1}(\mathbf{X}, t) = \gamma_{k1} y_k(t), \quad R_{k2} : \alpha_{k2}(\mathbf{X}, t) = \gamma_{k2} x_k(t),$$
$$R_{k3} : \alpha_{k3}(\mathbf{X}, t) = \gamma_{k3}, \quad R_{k4} : \alpha_{k4}(\mathbf{X}, t) = \gamma_{k4} y_k(t).$$

Diffusion is treated as a reaction in which a molecule jumps to one of its neighboring compartments at a constant rate. With periodic boundary conditions, diffusive jumps obey the following chain reactions:

$$A_1 \underset{\gamma}{\overset{\gamma}{\rightleftharpoons}} A_2 \underset{\gamma}{\overset{\gamma}{\rightleftharpoons}} A_3 \cdots \underset{\gamma}{\overset{\gamma}{\rightleftharpoons}} A_K \underset{\gamma}{\overset{\gamma}{\rightleftharpoons}} A_1,$$
$$B_1 \underset{\gamma}{\overset{\gamma}{\rightleftharpoons}} B_2 \underset{\gamma}{\overset{\gamma}{\rightleftharpoons}} B_3 \cdots \underset{\gamma}{\overset{\gamma}{\rightleftharpoons}} B_K \underset{\gamma}{\overset{\gamma}{\rightleftharpoons}} B_1.$$

where, $\gamma = D_m/h^2$. If considering no-flux boundary conditions, left jump of A_1 or B_1 and right jump of A_K or B_K will stay in its original compartment. Thus the *propensity functions* for diffusions are:

$$\alpha_{LA_k}(\mathbf{X}, t) = \gamma x_k(t), \quad \text{and} \quad \alpha_{RA_k}(\mathbf{X}, t) = \gamma x_k(t), \quad \text{for } 1 \leqslant k \leqslant K;$$
$$\alpha_{LB_k}(\mathbf{X}, t) = \gamma y_k(t), \quad \text{and} \quad \alpha_{RB_k}(\mathbf{X}, t) = \gamma y_k(t), \quad \text{for } 1 \leqslant k \leqslant K.$$

The system transfers from one state to another through reaction firing or diffusion jump. The net change vector of the state caused by one occurrence of reaction R_{kj} is denoted as $\widehat{\nu}_{kj}$ and then we have

$$R_{k1} : \widehat{\nu}_{k1} = \left(0, \ldots, 0, \underbrace{1}_{\text{kth}}, 0, \ldots, 0, \ldots, 0, \underbrace{-1}_{\text{(K+k)th}}, 0, \ldots, 0\right),$$
$$R_{k2} : \widehat{\nu}_{k2} = \left(0, \ldots, 0, \underbrace{-1}_{\text{kth}}, 0, \ldots, 0, \ldots, 0, \underbrace{1}_{\text{(K+k)th}}, 0, \ldots, 0\right),$$
$$R_{k3} : \widehat{\nu}_{k3} = \left(0, \ldots, 0, \underbrace{1}_{\text{(K+k)th}}, 0, \ldots, 0\right),$$
$$R_{k4} : \widehat{\nu}_{k4} = \left(0, \ldots, 0, \underbrace{-1}_{\text{(K+k)th}}, 0, \ldots, 0\right).$$

Similarly, we denote the net change vector of state induced by diffusion jump J_{LA_k}, J_{RA_k} of A_k as $\widehat{\nu}_{LA_k}$ and $\widehat{\nu}_{RA_k}$, and J_{LB_k}, J_{RB_k} of B_k as $\widehat{\nu}_{LB_k}$ and $\widehat{\nu}_{RB_k}$. We now develop a chemical master equation (CME) which corresponds to system of reactions and diffusions presented above:

$$\begin{aligned}\frac{\partial}{\partial t}P(\mathbf{X}, t) = &\sum_{k=2}^{K}[-\alpha_{LA_k}(\mathbf{X}, t)P(\mathbf{X}, t) + \alpha_{LA_k}(\mathbf{X} + \widehat{\nu}_{LA_k}, t)P(\mathbf{X} + \widehat{\nu}_{LA_k}, t)] \\ &+ \sum_{k=2}^{K}[-\alpha_{LB_k}(\mathbf{X}, t)P(\mathbf{X}, t) + \alpha_{LB_k}(\mathbf{X} + \widehat{\nu}_{LB_k}, t)P(\mathbf{X} + \widehat{\nu}_{LB_k}, t)] \\ &+ \sum_{k=1}^{K-1}[-\alpha_{RA_k}(\mathbf{X}, t)P(\mathbf{X}, t) + \alpha_{RA_k}(\mathbf{X} + \widehat{\nu}_{RA_k}, t)P(\mathbf{X} + \widehat{\nu}_{RA_k}, t)] \\ &+ \sum_{k=1}^{K-1}[-\alpha_{RB_k}(\mathbf{X}, t)P(\mathbf{X}, t) + \alpha_{RB_k}(\mathbf{X} + \widehat{\nu}_{RB_k}, t)P(\mathbf{X} + \widehat{\nu}_{RB_k}, t)] \\ &+ \sum_{k=1}^{K}\sum_{j=1}^{4}[-\alpha_{kj}(\mathbf{X}, t)P(\mathbf{X}, t) + \alpha_{kj}(\mathbf{X} + \widehat{\nu}_{kj}, t)P(\mathbf{X} + \widehat{\nu}_{kj}, t)].\end{aligned} \tag{6}$$

where $P(\mathbf{X}, t)$ is the probability density function.

3. Analysis for stochastic model

To analytically investigate the stochastic effect, the intrinsic noise in cell polarization process will be studied through approximating the power spectrum. Analytical power spectrum can be used to find the frequency distribution and predict the behavior of inherent fluctuations near the deterministic steady state [22–24]. For example, the linear noise approximation and the power spectrum have been used to investigate the stochastic oscillations of intracellular calcium and showed the intrinsic noise can derive the emergence of stochastic waves [24].

In this section, we first apply linear noise approximation to obtain a Langevin equation for chemical reactions and diffusions. Then Fourier transform is utilized to derive the theoretical approximation for the power spectrum.

3.1. Langevin equation derivation by linear noise approximation

Here we approximate the number of molecules in the kth compartment as follows:

$$\frac{x_k}{\Lambda} \approx a_k(t) + \frac{\xi_k}{\sqrt{\Lambda}}, \tag{7a}$$

$$\frac{y_k}{\Lambda} \approx b_k(t) + \frac{\eta_k}{\sqrt{\Lambda}}, \tag{7b}$$

where Λ is the volume of each compartment; the functions $a_k(t)$ and $b_k(t)$ are the macroscopic parts of the concentration of active and inactive molecules in the kth compartment; the terms ξ_k and η_k are real random numbers, which measure the fluctuations around $a_k(t)$ and $b_k(t)$, respectively. The fluctuations are assumed to have a zero mean and the covariances will be determined by the equation provided later. The corresponding transition probability of each reaction and diffusion will be scaled by Λ. In the following calculation, we use a function $G(x_k/\Lambda, y_k/\Lambda)$ to represent $g_{on}(N - \sum_k (x_k + y_k))Q(x_k/\Lambda, y_k/\Lambda)$.

Recall that we aim to capture the dynamics of fluctuations and thus the probability distribution is expressed in terms of (ξ_k, η_k, t) by $\Pi(\xi_k, \eta_k, t) = \Lambda^{K/2} P(x_k(a_k(t), \xi_k), y_k(b_k(t), \eta_k), t)$. By making the systematic expansion of the master Eq. (6) and scaling the time variable by $t = \Lambda\tau$ to balance the terms on both sides, we obtain

$$\sum_{k=1}^{K} \left(\frac{\partial \Pi}{\partial \tau} \frac{1}{\Lambda} - \frac{\partial \Pi}{\partial \xi_k} \frac{1}{\sqrt{\Lambda}} \dot{a}_k - \frac{\partial \Pi}{\partial \eta_k} \frac{1}{\sqrt{\Lambda}} \dot{b}_k \right) = \sum_{k=1}^{K} [A + B + C + D], \tag{8}$$

where

$$\begin{aligned}
A = {} & \frac{1}{\sqrt{\Lambda}} \left(\frac{\partial}{\partial \xi_k} - \frac{\partial}{\partial \eta_k} \right) (k_{off} a_k - F b_k) \Pi \\
& + \frac{1}{\Lambda} \left(\frac{\partial}{\partial \xi_k} - \frac{\partial}{\partial \eta_k} \right) [k_{off} \xi_k - (F \eta_k + F' \xi_k b_k)] \Pi + \frac{1}{2\Lambda} \left(\frac{\partial^2}{\partial \eta_k^2} + \frac{\partial^2}{\partial \xi_k^2} - 2 \frac{\partial}{\partial \eta_k} \frac{\partial}{\partial \xi_k} \right) (k_{off} a_k + F b_k) \Pi, \\
B = {} & \frac{1}{\sqrt{\Lambda}} \frac{\partial}{\partial \eta_k} (g_{off} b_k - G) \Pi \\
& + \frac{1}{\Lambda} \frac{\partial}{\partial \eta_k} \left[g_{off} \eta_k - \left(\frac{\partial G}{\partial a_k} \xi_k + \frac{\partial G}{\partial b_k} \eta_k \right) \right] \Pi + \frac{1}{2\Lambda} \frac{\partial^2}{\partial \eta_k^2} (G + g_{off} b_k) \Pi, \\
C = {} & \gamma \sum_{j \in \{k-1, k+1\}} \left[\frac{1}{\sqrt{\Lambda}} \left(\frac{\partial}{\partial \xi_k} - \frac{\partial}{\partial \xi_j} \right) (a_k - a_j) \Pi \right. \\
& \left. + \frac{1}{\Lambda} \left(\frac{\partial}{\partial \xi_k} - \frac{\partial}{\partial \xi_j} \right) (\xi_k - \xi_j) \Pi + \frac{1}{2\Lambda} \left(\frac{\partial^2}{\partial \xi_k^2} + \frac{\partial^2}{\partial \xi_k^2} - 2 \frac{\partial}{\partial \xi_k} \frac{\partial}{\partial \xi_k} \right) (a_k + a_j) \Pi \right], \\
D = {} & \gamma \sum_{j \in \{k-1, k+1\}} \left[\frac{1}{\sqrt{\Lambda}} \left(\frac{\partial}{\partial \eta_k} - \frac{\partial}{\partial \eta_j} \right) (b_k - b_j) \Pi \right. \\
& \left. + \frac{1}{\Lambda} \left(\frac{\partial}{\partial \eta_k} - \frac{\partial}{\partial \eta_j} \right) (\eta_k - \eta_j) \Pi + \frac{1}{2\Lambda} \left(\frac{\partial^2}{\partial \eta_k^2} + \frac{\partial^2}{\partial \eta_k^2} - 2 \frac{\partial}{\partial \eta_k} \frac{\partial}{\partial \eta_k} \right) (b_k + b_j) \Pi \right].
\end{aligned}$$

and F' is the derivative of positive feedback function evaluated at a_k.

Comparing the two sides of Eq. (8) with same order of $1/\sqrt{\Lambda}$, it contributes to the mean-field equations

$$\begin{aligned}
\dot{a}_k &= \frac{D_m}{h^2} \Delta a_k + F b_k - k_{off} a_k, \\
\dot{b}_k &= \frac{D_m}{h^2} \Delta b_k - F b_k + k_{off} a_k + G - g_{off} b_k.
\end{aligned}$$

which agrees with aforementioned deterministic system (1a)–(1b). Comparing the two sides with order of $1/\Lambda$, it leads to the Fokker-Planck equation [25]:

$$\frac{\partial \Pi}{\partial \tau} = \sum_{k=1}^{K} \left[-\sum_{r=1}^{2} \frac{\partial}{\partial \phi_{r,k}} \left(\sum_{m=1}^{2} J_{rm,k} \phi_{m,k} \Pi \right) + \frac{1}{2} \sum_{r,l=1}^{2} \sum_{j=k-1}^{k+1} \frac{\partial}{\partial \phi_{l,k}} \frac{\partial}{\partial \phi_{r,k}} \left(M_{rlj,k} \Pi \right) \right], \tag{9}$$

where $(\phi_{1,k}, \phi_{2,k}) = (\xi_k, \eta_k)$; $J_{rm,k}$, which is the element of the 2×2 matrix $\mathbf{J}_k$, is given by

$$\mathbf{J}_k = \begin{pmatrix} F' b_k - k_{off} + \gamma \Delta & F \\ -F' b_k + k_{off} + \frac{\partial G}{\partial a_k} & -F - g_{off} + \frac{\partial G}{\partial b_k} + \gamma \Delta \end{pmatrix},$$

where the discrete Laplacian operator works as $\Delta a_k = a_{k-1} - 2a_k + a_{k+1}$ in one-dimensional space and the 2×2 block matrix $\mathbf{M}_k$ is defined as

$$\mathbf{M}_{11\,j,k} = \begin{cases} -\gamma(a_k + a_{k-1}) & \text{if } j = k-1, \\ \gamma(2a_k + a_{k-1} + a_{k+1}) + (Fb_k + k_{off}a_k) & \text{if } j = k, \\ -\gamma(a_k + a_{k+1}) & \text{if } j = k+1, \end{cases}$$

$$\mathbf{M}_{22\,j,k} = \begin{cases} -\gamma(b_k + b_{k-1}) & \text{if } j = k-1, \\ \gamma(2b_k + b_{k-1} + b_{k+1}) + Fb_k + k_{off}a_k + G + g_{off}b_k & \text{if } j = k, \\ -\gamma(b_k + b_{k+1}) & \text{if } j = k+1, \end{cases}$$

$$\mathbf{M}_{12\,j,k} = \begin{cases} 0 & \text{if } j = k-1, \\ -(Fb_k + k_{off}a_k) & \text{if } j = k, \\ 0 & \text{if } j = k+1, \end{cases}$$

$$\mathbf{M}_{21\,j,k} = \mathbf{M}_{12\,j,k} \text{ for } j = k-1, k, k+1.$$

Although Fokker-Planck Eq. (9) provides the information of probability distribution, it is not so powerful for analysis. Therefore, we consider the corresponding Langevin equation [25] which formulates with actual stochastic variable $\phi_{r,k}$ for $r = 1, 2$ and $k = 1, 2, \ldots, K$:

$$\frac{d}{d\tau}\phi_{r,k}(\tau) = \sum_{l=1}^{2} J_{rl,k}\phi_{l,k}(\tau) + \mu_{r,k}(\tau), \tag{10}$$

where $\mu_{r,k}(\tau)$ is a noise term having a Gaussian probability distribution with the first and second moments: $\langle \mu_{r,k}(\tau) \rangle = 0$, and $\langle \mu_{r,k}(\tau), \mu_{l,j}(\tau') \rangle = M_{rlj,k}\delta(\tau - \tau')$. In the second moment, $M_{rlj,k}$ measures the strength of the noise and the delta function claims that no correlation exists between two distinct time τ and τ', that is, the Fourier transform of this correlation function is frequency-independent.

3.2. Power spectrum estimation of fluctuation

Langevin equation in (10) allows us to take Fourier transform conveniently and a power spectrum of fluctuation can be deduced after the transformation [26]. In Langevin Eq. (10), both $\mathbf{J}_k$ and $\mathbf{M}_k$ are time-dependent and space-dependent. Here we focus on the fluctuations around homogeneous steady state, and thus $\mathbf{J}_k$ and $\mathbf{M}_k$ will be evaluated at (a^*, b^*) and we let them be $\mathbf{J}_k^*$ and $\mathbf{M}_k^*$. Therefore, elements $J_{rl,k}^*$ with r and l referring to molecule species in matrix $\mathbf{J}_k^*$ are as follows: $J_{11,k}^* = F'b^* - k_{off} + \gamma\Delta$, $J_{12,k}^* = F$, $J_{21,k}^* = -F'b^* + k_{off} + \frac{\partial G}{\partial a_k}$, $J_{22,k}^* = -F - g_{off} + \frac{\partial G}{\partial b_k} + \gamma\Delta$. From now on, F, F', $\frac{\partial G}{\partial a_k}$ and $\frac{\partial G}{\partial b_k}$ are the values evaluated at (a^*, b^*) and entries in $\mathbf{M}_k^*$ are defined similarly. With the definition of $\mathbf{M}_k$ given in (9), matrix $\mathbf{M}_k^*$ has the following compact form:

$$\mathbf{M}_{rlj,k}^* = \mathbf{M}_{rl}^{(0)}\delta_{|k-j|,0} + \mathbf{M}_{rl}^{(1)}\delta_{|k-j|,1}, \tag{11}$$

where

$$\mathbf{M}^{(0)} = \begin{pmatrix} 4\gamma a^* + (Fb^* + k_{off}a^*) & -(Fb^* + k_{off}a^*) \\ -(Fb^* + k_{off}a^*) & 4\gamma b^* + Fb^* + k_{off}a^* + G + g_{off}b^* \end{pmatrix},$$

$$\mathbf{M}^{(1)} = \begin{pmatrix} -2\gamma a^* & 0 \\ 0 & -2\gamma b^* \end{pmatrix},$$

$$\delta_{i,j} = \begin{cases} 1 & \text{if } i = j, \\ 0 & \text{otherwise.} \end{cases}$$

Here we take the temporal and spatial Fourier transform of a generic function $f(\cdot)$ with $\hat{f}(\omega) = \int_0^{+\infty} f(t)e^{-i\omega t}\,dt$ and $\hat{f}(k_0) = \sum_{x=0}^{+\infty} f(x)e^{-ik_0x}$ where $\hat{(\cdot)}$ stands for Fourier transform. Thus, after applying spatial and temporal Fourier transform to Eq. (10), it gives

$$i\omega\hat{\phi}_r(k_0, \omega) = \sum_{l=1}^{2} \hat{J}_{rl}^*(k_0)\hat{\phi}_l(k_0, \omega) + \hat{\mu}_r(k_0, \omega), \tag{12}$$

where $\langle \hat{\mu}_r(\omega)\overline{\hat{\mu}_l(\omega)} \rangle = \hat{M}_{rl}^*$. k_0 is the angular frequency which is continuous and lies in the $[0, 2\pi]$ and ω is the frequency emerging from temporal Fourier transform. For the elements $\hat{J}_{rl}^*$, the discrete Laplacian Δ is changed to $\hat{\Delta}$. In a one-dimensional space, discrete Laplacian is transformed to $\hat{\Delta} = 2(\cos(k_0) - 1)$ [27] and thus the matrix in Eq. (11) is replaced by the form:

$$\hat{\mathbf{M}}^* = (\mathbf{M}^{(0)} + 2\mathbf{M}^{(1)}) + \mathbf{M}^{(1)}\hat{\Delta},$$

where the elements are $\hat{M}_{11}^* = (Fb^* + k_{off}a^*) - 2\gamma a^*\hat{\Delta}$, $\hat{M}_{12}^* = \hat{M}_{21}^* = -(Fb^* + k_{off}a^*)$, $\hat{M}_{22}^* = Fb^* + k_{off}a^* + G + g_{off}b^* - 2\gamma b^*\hat{\Delta}$. Note that, for simplicity, we have denoted $(\phi_{1,k}, \phi_{2,k}) = (\xi_k, \eta_k)$. We are now in position to present the power spectrum of the Fourier-transformed fluctuations $\hat{\phi}_1(k_0, \omega)$ and $\hat{\phi}_2(k_0, \omega)$. Analytical power spectra for active molecule a and inactive molecule b are defined by

$$P_1(k_0, \omega) = \langle |\hat{\phi}_1(k_0, \omega)|^2 \rangle, \quad P_2(k_0, \omega) = \langle |\hat{\phi}_2(k_0, \omega)|^2 \rangle.$$

Based on the definition, the explicit form of $P_1(k_0, \omega)$ and $P_2(k_0, \omega)$ can be derived and detailed derivations are provided in Appendix B. After some algebraic manipulations, it yields the following explicit forms

$$P_1(k_0,\omega) = \frac{C_1(k_0) + \hat{M}^*_{11}\omega^2}{(\omega^2 - \Theta^2)^2 + \Gamma^2\omega^2},$$
$$P_2(k_0,\omega) = \frac{C_2(k_0) + \hat{M}^*_{22}\omega^2}{(\omega^2 - \Theta^2)^2 + \Gamma^2\omega^2}, \tag{13}$$

where

$$\Theta = \sqrt{\det(\hat{\mathbf{J}}^*)}, \quad \Gamma = -\mathrm{tr}\,(\hat{\mathbf{J}}^*),$$
$$C_1(k_0) = \hat{M}^*_{11}(\hat{J}^*_{22})^2 + \hat{M}^*_{22}(\hat{J}^*_{12})^2 - 2\hat{M}^*_{12}\hat{J}^*_{12}\hat{J}^*_{22},$$
$$C_2(k_0) = \hat{M}^*_{22}(\hat{J}^*_{11})^2 + \hat{M}^*_{11}(\hat{J}^*_{21})^2 - 2\hat{M}^*_{12}\hat{J}^*_{21}\hat{J}^*_{11}.$$

The profile of power spectrum gives information about the distribution of fluctuation at different frequencies. Therefore, in the following section, we will use the expressions of power spectrum in Eq. (13) to analyze and predict the conditions for pattern formation.

4. Numerical results

To verify the aforementioned models, some numerical simulations for the system of RDEs and SSA are studied here. In the system of RDEs, we adopt a second-order central difference approximation for the Laplacian operator, Riemann sum for the definite integrals, Adams-Moulton predictor-corrector method with adaptive step size for the temporal discretization, and periodic boundary conditions for the boundaries. Note that we also employed the no-flux boundary conditions and no major differences were observed on the results compared to periodic boundary conditions. For SSA, a detailed algorithm for stochastic simulation is proposed in Appendix C. Experimental observations [28] demonstrate that a critical event marking the success of cell polarity is the localization of signaling molecules to the specific region of the membrane. In our numerical simulations, the emergence of cell polarity is determined by whether 15% of the continuous interval contains $\geqslant$ 50% active signaling molecules on the membrane [16]. For one-dimensional simulations, the number of spatial points is 200 and the temporal step Δt is 1×10^{-3} min. Initial conditions for simulations are defined as $a(x,0) = 0$ and $b(x,0) = 0.3(1 + 0.2\eta(x))$ where $\eta(x)$ is a function of uniformly distributed random number from 0 to 1.

4.1. Feedback in the form of quadratic function

Fig. 1 ABC shows the distribution profiles of active molecules obtained by solving RDEs. In the simulations of Fig. 1AB, the stable localization of active molecules can be achieved within 120 mins, which indicates the emergence of cell polarity; in the simulation of Fig. 1C, the solution becomes homogeneous at the end and thus it fails to exhibit the polarization. Stochastic simulations are also obtained by performing SSA and the results at $t = 120$ mins are displayed in Fig. 1DEF. The corresponding spatio-temporal dynamics are shown in Fig. 2BC. Although distribution profiles show much noisy localization at 120 mins, it is remarkable that the stochastic system still produces localization at $\Omega = 93, N = 481$ (see Fig. 1F and C) where RDEs fail (see Fig. 1C).

The discrepancy at parameter setting $\Omega = 93, N = 481$ (Fig. 1C and F) indicates that the parameter regimes for achieving cell polarity are different in deterministic and stochastic systems. It is consistent with the observations from some previous studies [13,17,29]. Therefore, we further investigate the effect of fluctuation on polarity establishment by analyzing the Turing stability in the deterministic system and power spectrum in the stochastic system.

According to the derivation of the power spectrum, we know that the frequency ω mainly affects the term $e^{-i\omega}$. Therefore, the power spectrum is periodic regarding ω with a period 2π. Moreover, due to the property of even function, the information in the range $[0, \pi]$ is sufficient for analysis. To measure the relative change of the power spectrum, $P(k_0,\omega)$ is normalized by $P(0,0)$. In the analysis of power spectrum, the profile captured by $P_1(k_0,\omega)$ or $P_2(k_0,\omega)$ is utilized to measure the effect of random fluctuations [23,30]. It gives a complete representation of how the variance of fluctuation is distributed at different frequencies. If there is no order of fluctuations, the profile will be flat or have a peak at wavenumber zero (see Fig. 3AB); otherwise, it will have at least one peak at non-zero wavenumber $k_0 \neq 0$ and zero temporal frequency $\omega = 0$ (see Fig. 3CD). Here non-zero wavenumber indicates the non-trivial spatial structure. In contrast, if the power spectrum presents a peak at zero wavenumber $k_0 = 0$ and non-zero temporal frequency $\omega \neq 0$, it represents the global oscillation.

The parameter region for achieving cell polarity predicted by the power spectrum is shown in Fig. 4A. It is a phase diagram of carrying capacity Ω and the total number of molecules N. The power spectrum analysis suggests that when the total number of the molecules is small (less than 93), the localization loses. As the amount increases, larger carrying capacity is needed to ensure the onset of localization. Moreover, in comparison with the simulation results of SSA (see Fig. 4B), the parameter range obtained by SSA is mostly in accordance with the prediction of the power spectrum in spite of variations observed at the boundary (the blue region in Fig. 4B).

To see the difference of parameter regimes between deterministic and stochastic systems, Fig. 4C compares the results predicted by RDEs and SSA where stochastic method leads to a broader parameter region for the emergence of cell polarity. This result supports that existing intrinsic noise increases robustness during the polarization process. In this analysis, we observe that an analytical expression of the power spectrum provides an efficient and accurate method to investigate the parameter region for achieving the Turing pattern instead of the time-consuming SSA.

4.2. Feedback in the form of linear function

Here we also consider a simple feedback form, the linear feedback function, which means that function (2) has no cooperativity: $F(a) = k_{11} + k_{12}a$. Altschuler et al. [9] have proposed that the linear positive feedback is insufficient to establish localization in the deterministic model. Our theory based on linear stability analysis provides the conditions which support the failure in the deterministic system (see Appendix D and [21]).

In the stochastic model, we set $\Omega = 93$, $N = 200$, $k_{11} = 20\,\mathrm{min}^{-1}$, varied k_{12}, and other parameters are used as Table 1. With weak feedback strength, $k_{12} = 0.987\,\mathrm{min}^{-1}$ and $k_{12} = 10\,\mathrm{min}^{-1}$, it fails to establish cell polarity. Whereas with much stronger strength $k_{12} = 40\,\mathrm{min}^{-1}$ and $k_{12} = 100\,\mathrm{min}^{-1}$, active molecules successfully produce the pattern (see Fig. 5 left column). More importantly, prediction by power spectrum method is consistent with this observation. Specifically, it displays peak profiles at non-zero wavenumber when $k_{12} = 40\,\mathrm{min}^{-1}$ and $k_{12} = 100\,\mathrm{min}^{-1}$ and no peak profile is observed when $k_{12} = 0.987\,\mathrm{min}^{-1}$ and $k_{12} = 10\,\mathrm{min}^{-1}$ (see Fig. 5 right column). Thus this verifies that even with a linear feedback regulation in polarizing process, the prediction by power spectrum could be useful to determine the condition for achieving symmetry breaking.

4.3. Feedback in the form of Hill function

With the feedback function in Eq. (2), the amplification strength increases fast with the increasing concentrated cluster, whereas the saturation which represses the recruiting strength may exist in the feedback loop. Therefore the feedback regulation is described as a

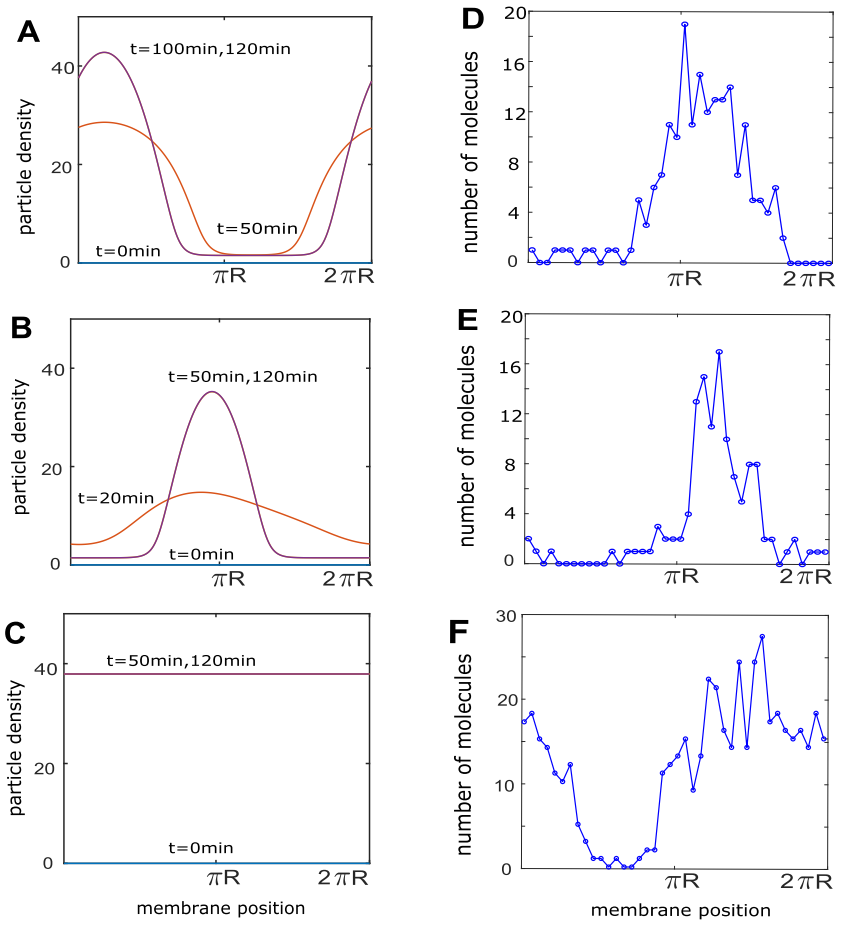

Fig. 1. Distribution profile of active molecules in deterministic system (left column) and stochastic system (right column) with feedback in the form of quadratic function. (A) and (D) $\Omega = 93$, $N = 201$; (B) and (E) $\Omega = 173$, $N = 131$; (C) and (F) $\Omega = 93$, $N = 481$.

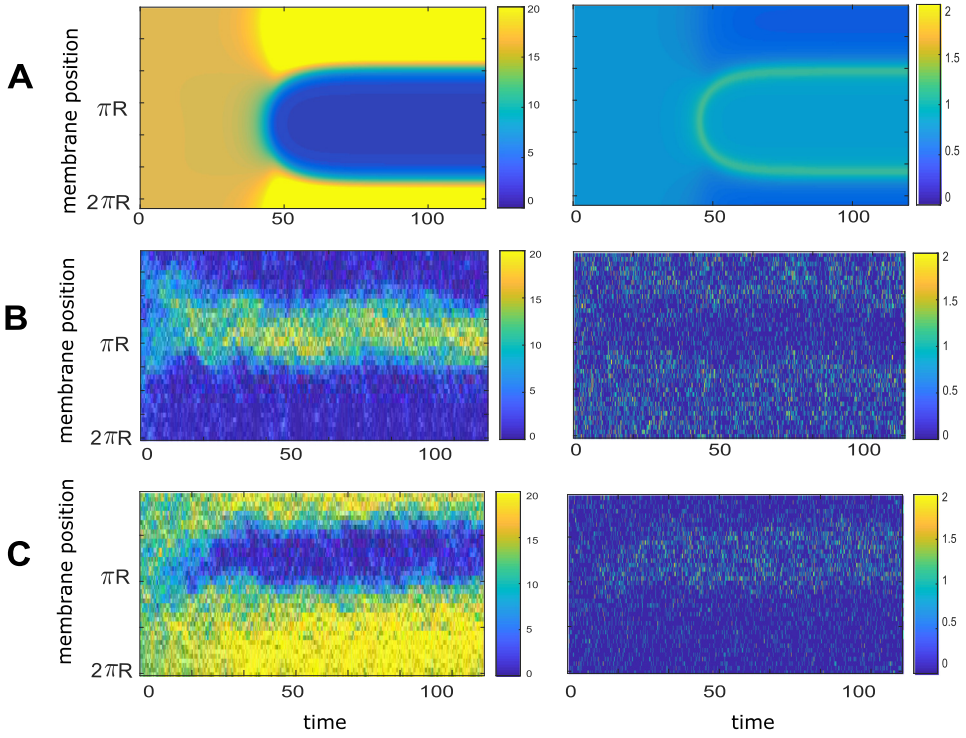

Fig. 2. Spatio-temporal dynamics of active molecules in deterministic system (A) and stochastic system (B and C) with quadratic feedback function. Color bar shows the number of molecules in each compartment on membrane. (A) and (B) $\Omega = 93$, $N = 201$; (C) $\Omega = 93$, $N = 481$. $\sigma_1 D_m = 0.0375 \mu m^2\ \mathrm{min}^{-1}$. (For interpretation of the references to color in this figure legend, the reader is referred to the web version of this article.)

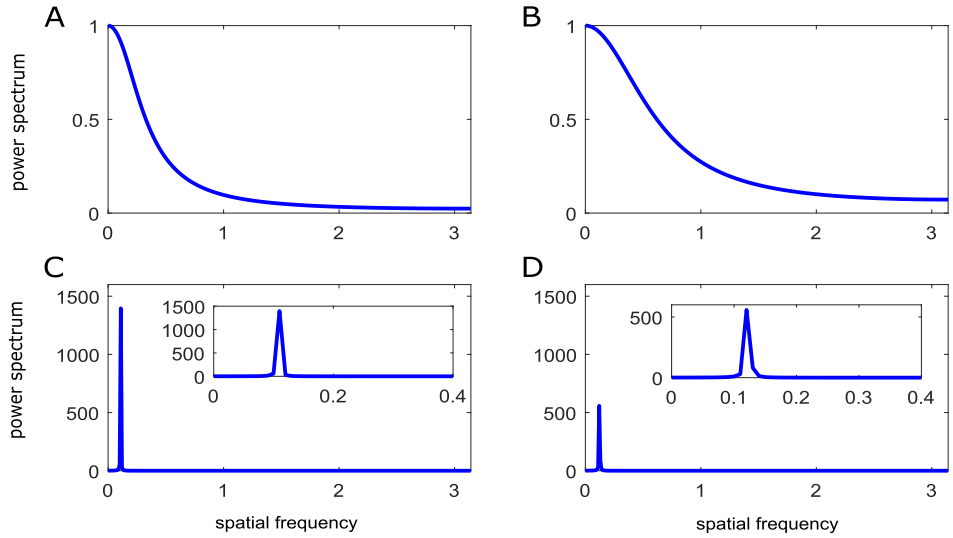

Fig. 3. Power spectrum profiles at different carrying capacity Ω and total number of molecules N. (A) $\Omega = 53$, $N = 481$; (B) $\Omega = 93$, $N = 51$; (C) $\Omega = 93$, $N = 481$; (D) $\Omega = 53$, $N = 301$. Horizontal axis denotes the spatial frequency $k_0 \in [0, \pi]$; vertical axis denotes the normalized power spectrum of active molecules $P_1(k_0, \omega)$.

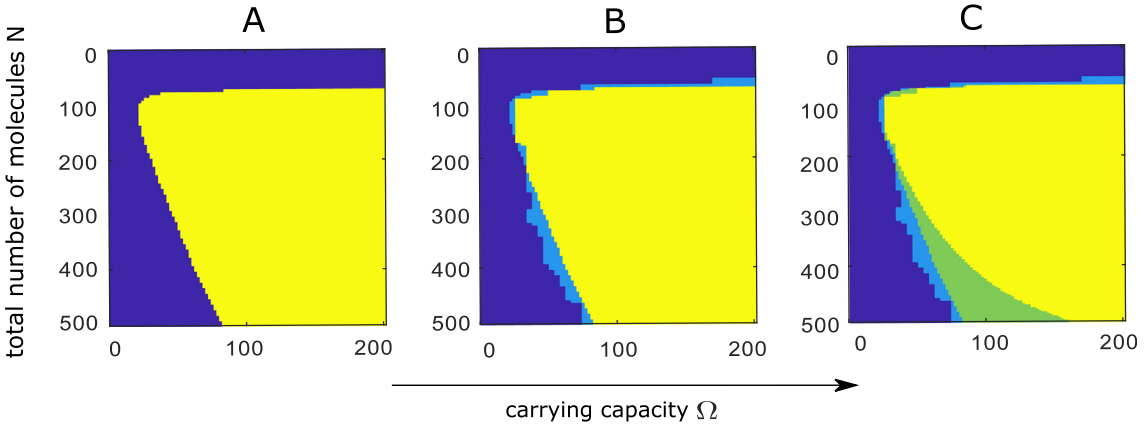

Fig. 4. Phase diagram of carrying capacity Ω and total number of molecules N with feedback in the form of quadratic function. (A) Parameter region (in yellow) predicted by the power spectrum. (B) The difference in parameter regions obtained by the power spectrum and SSA. (C) The difference in parameter regions obtained by the power spectrum, RDEs, and SSA. Yellow region represents the prediction of power spectrum; purple region denotes failure of the occurrence; blue region in B is the difference between the power spectrum and SSA; green region in C denotes the difference between power spectrum and RDEs. (For interpretation of the references to color in this figure legend, the reader is referred to the web version of this article.)

Hill function (3) and considering $n = 2$:

$$F(a) = k_{21} + \frac{k_{22}a^2}{k_{23}^2 + a^2}.$$

where the saturation constant k_{23} is introduced. When the density of Cdc42-GTP is high, recruiting power will be limited and the recruiting strength will saturate to a maximal level at k_{22}.

Based on the linear stability analysis and analytical power spectrum, we will explore how this saturation in recruitment will affect the parameter regime for polarity establishment. With the above derived Turing instability criteria, the sufficient and necessary conditions for achieving pattern formation are as follows:

$$\frac{2k_{22}k_{23}^2a^*}{(k_{23}^2 + a^{*2})^2}b^* - k_{off} - \frac{g_{on}\frac{N-a^*L-b^*L}{\Omega} + g_{on}QL}{g_{on}\frac{N-a^*L-b^*L}{\Omega} + g_{on}QL + g_{off}}\left(k_{21} + \frac{k_{22}a^{*2}}{k_{23}^2 + a^{*2}}\right) < 0, \tag{14}$$

and

$$-\sigma_1 D_m + \frac{2k_{22}k_{23}^2a^*}{(k_{23}^2 + a^{*2})^2}b^* - k_{off} - \frac{\sigma_1 D_m + g_{on}\frac{N-a^*L-b^*L}{\Omega}}{\sigma_1 D_m + g_{on}\frac{N-a^*L-b^*L}{\Omega} + g_{off}}\left(k_{21} + \frac{k_{22}a^{*2}}{k_{23}^2 + a^{*2}}\right) > 0. \tag{15}$$

Conditions for the emergence of cell polarity in (14)–(15) are made use of to disclose the dependencies on the carrying capacity and total number of molecules (see Fig. 6). It can be seen that the available parameter region in the system with Hill function (in yellow) is completely covered by the one with quadratic feedback function (see Fig. 6A). It implies that the limit on local recruitment of active signaling molecules results in a smaller parameter region for pattern formation. In comparison with power spectrum prediction in Fig. 6B, that localization only occurs in the stochastic regime is also witnessed although this available range (in turquoise) is narrow. In particular, the region for the Turing pattern predicted by the power spectrum only extends a little bit along the boundary. Repression due to Hill function could not help to amplify the fluctuation such that only a rather small difference is observed. Two points, $\Omega = 93$, $N = 351$ and $\Omega = 193$, $N = 426$, are chosen from this gap area and their corresponding power spectrum profiles are illustrated in Fig. 6CD. The peak pro-

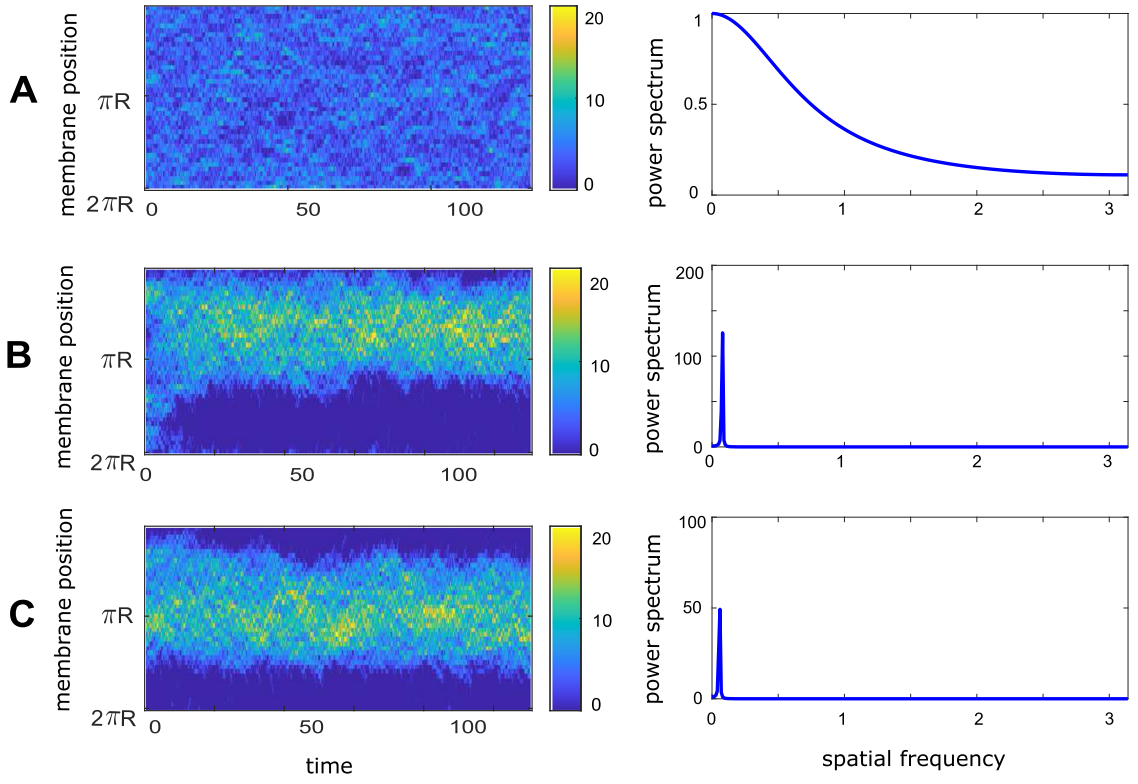

Fig. 5. Stochastic spatio-temporal dynamics of active molecules (left column) and the corresponding power spectrum profiles (right column) with feedback in the form of linear function. Color bar shows the number of molecules in each compartment on membrane. (A) $k_{12} = 0.987\,\text{min}^{-1}$; (B) $k_{12} = 40\,\text{min}^{-1}$; (C) $k_{12} = 100\,\text{min}^{-1}$. $\Omega = 93$, $N = 201$, $\sigma_1 D_m = 0.0375\mu m^2\,\text{min}^{-1}$.

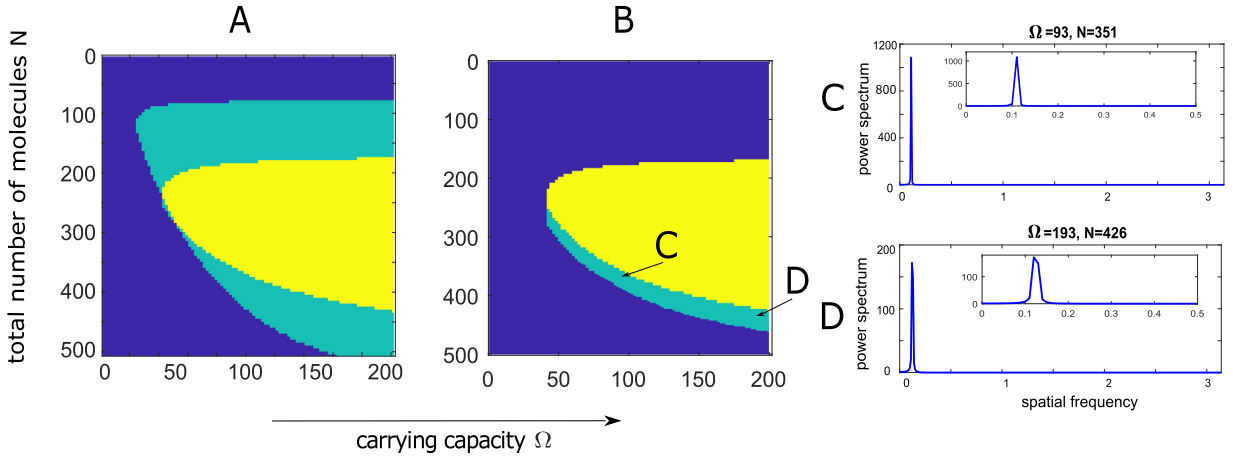

Fig. 6. Phase diagram of carrying capacity Ω and total number of molecules N with feedback in the form of Hill function. (A) Difference in the parameter regions in system with Hill function and quadratic feedback function. (B) The difference in the parameter regions obtained by RDEs and power spectrum. Yellow area denotes the occurrence of Turing pattern; purple area represents failure of the occurrence. Turquoise area in A represents the region where the system fails to produce pattern with Hill function but succeeds with quadratic function; turquoise region in B represents the region where RDEs fails but power spectrum prediction succeeds. And points C and D are picked from this gap area with (C) $\Omega = 93$, $N = 351$; (D) $\Omega = 193$, $N = 426$. The peak profiles of power spectrum at nonzero spatial frequency confirm the existence of random fluctuation which therefore indicates the emergence of cell localization. (For interpretation of the references to color in this figure legend, the reader is referred to the web version of this article.)

files at nonzero spatial frequency confirm the existence of random fluctuation, which indicates the emergence of cell localization.

4.4. Comparison of localization behaviors with different limitations of recruitment

If there is no constraint on the recruitment of cytoplasmic inactive signaling molecules, carrying capacity on membrane is large enough ($Q = 1$ as $\Omega \to +\infty$). In this case, Turing instability conditions will be

$$\frac{2k_{22}k_{23}^2a^*}{(k_{23}^2+a^{*2})^2}b^* - k_{off} - \frac{g_{on}L}{g_{on}L+g_{off}}\left(k_{21}+\frac{k_{22}a^{*2}}{k_{23}^2+a^{*2}}\right) < 0,$$

and

$$-\sigma_1 D_m + \frac{2k_{22}k_{23}^2a^*}{(k_{23}^2+a^{*2})^2}b^* - k_{off} - \frac{\sigma_1 D_m}{\sigma_1 D_m + g_{off}}\left(k_{21}+\frac{k_{22}a^{*2}}{k_{23}^2+a^{*2}}\right) > 0.$$

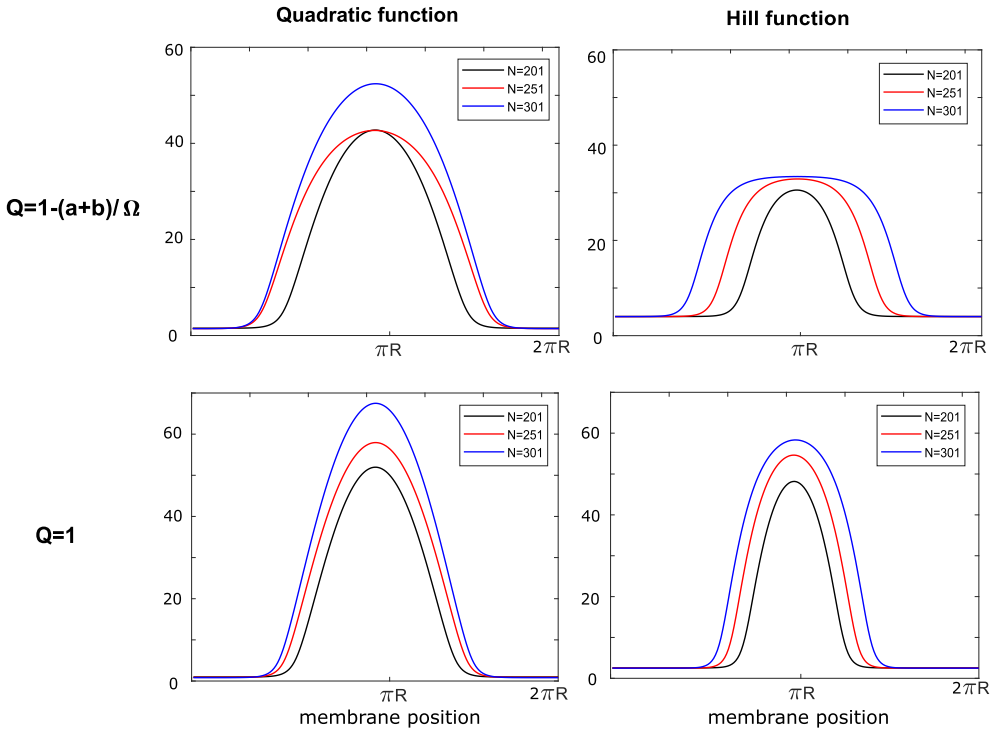

Fig. 7. Distribution profile of active molecules with quadratic feedback function (left column) or Hill function (right column). Upper panel represents the system with local carrying capacity $Q(a,b)=1-\frac{a+b}{\Omega}$ (numerically $\Omega=93$). Lower panel represents the system without carrying capacity, i.e., $Q=1$. In the system with carrying capacity, we calculated the Q value at peak. With quadratic feedback function, $Q(a,b)$ is 0.53, 0.53 and 0.45 as total number of molecules increases from 201, 251 to 301. With Hill function, $Q(a,b)$ is 0.61, 0.58 and 0.58 as total number of molecules increases from 201, 251 to 301. Other parameters not specified are used according to Table 1.

Table 1
Parameters used in the model; the diffusion rate, recruitment rate and dissociation rate of inactive molecules, and deactivation rate of active molecules are taken from Lo et al. [21].

Parameter	Value/Unit	Description
a	mol μm^{-2}	Concentration of active molecules
b	mol μm^{-2}	Concentration of inactive molecules
D_m	0.15 $\mu m^2\,\mathrm{min}^{-1}$	Diffusion rate of molecules
R	2 μm	Yeast cell radius
g_{on}	20 $\mu m^{-2}\,\mathrm{min}^{-1}$	Recruitment rate of inactive molecules
g_{off}	9 min^{-1}	Dissociation rate of inactive molecules
k_{off}	10 min^{-1}	Deactivation rate of active molecules
n	1 or 2	Degree of cooperativity
k_{11}	20 min^{-1}	Basal activation rate of Cdc42 in Eq. (2)
k_{12}	0.987 [mol $\mu m^{-2}]^{-n}\mathrm{min}^{-1}$	Activation coefficient through cooperative feedback in Eq. (2)
k_{21}	5 min^{-1}	Basal activation rate in Eq. (3)
k_{22}	200 min^{-1}	Feedback activation coefficient in Eq. (3)
k_{23}	40 mol μm^{-2}	Saturation parameter in Eq. (3)
N	–	Total number of molecules
Ω	–	Local carrying capacity on cell membrane

Based on these conditions, numerical simulation results (which are not given here) demonstrate that if the system incorporates with quadratic feedback form, the total amount of signaling molecules N has to be larger than 76 to yield Turing pattern. In contrast, if the system is equipped with Hill function, the total amount of signaling molecules N should be higher than 171. Furthermore, in previous section considering the local carrying capacity as $Q(a,b)=1-\frac{a+b}{\Omega}$, the least number of molecules ensuring Turing pattern is around 76 and 171 in system with quadratic function and Hill function respectively when Ω is larger than 90 (see Fig. 6A). In a word, this reveals that the existence of recruiting limitation does not influence the lower bound of the number of molecules for obtaining a pattern. On the other hand, the limitation on recruitment inhibits the magnitude of concentrated Cdc42-GTP cluster (see Fig. 7 upper panel). Without the limitation on recruitment, i.e., $Q=1$, the localized cluster is much sharper than the case incorporating $Q(a,b)=1-\frac{a+b}{\Omega}$. Hence, when the recruitment of active signaling molecules is limited by saturation, the lowest number of signaling molecules for achieving polarity may not be affected but the magnitude of the localized cluster is repressed.

5. Conclusion

In this paper, we formulated deterministic and stochastic models with non-local kinetics to describe the cell polarization process. Our model consists of active and inactive signaling molecules where the recruitment of inactive molecules from the whole cytoplasm is taken into account. Parameter regime and localization behavior were compared and discussed for the models with different positive feedback forms. We used numerical method SSA and the analysis of the power spectrum to approximate the parameter ranges and compared the results obtained by Turing instability conditions.

Our results suggest that the stochastic fluctuations in the model with quadratic or Hill function form feedback can extend the parameter regime for achieving cell polarization. A good agreement between the prediction of the power spectrum and the simulations of SSA was observed, and this result allows us to use the power spectrum to effectively predict the regimes instead of implementing the time-consuming SSA. Also, the model with Hill function feedback form yields a smaller parameter regime than that with quadratic feedback function. Moreover, considering systems with and without local carry capacity on recruiting signaling molecules, Hill function feedback might repress the magnitude of localization. The differences in feedback function illustrate that Turing and wave-pinning mechanisms react distinctly even with the intrinsic fluctuation, which is also one of the contributions of this paper.

The simplified model used by assuming the cell as a circle while unintentionally neglecting the cell shape or curvature may bring some limitations to this study as the cell geometry also affects the pattern formation, as pointed out by recent studies [14,31]. Therefore, our next work is intended to explore the polarization process in a system with varied cell geometries.

Declaration of Competing Interest

The authors declare that they have no known competing financial interests or personal relationships that could have appeared to influence the work reported in this paper.

CRediT authorship contribution statement

Yue Liu: Writing - review & editing, Visualization. **Wing-Cheong Lo:** Funding acquisition, Supervision, Writing - review & editing.

Acknowledgements

This work is supported by grants from the Research Grants Council of Hong Kong Special Administrative Region [Project No. CityU 11303117]. The first author is grateful to the University Grants Committee (UGC) in Hong Kong for the financial support.

Appendix A. Turing instability analysis

First, in homogeneous system with uniform density over whole space, the diffusion terms $\nabla^2 a$ and $\nabla^2 b$ vanish. Only reaction terms are remained and also balanced for a and b. Note that since a^* is homogeneous over space, $\widetilde{a^*} = \int a^*\ dS = a^* L$ and $\widetilde{b^*} = \int b^*\ dS = b^* L$ in one dimension. The steady state solution (a^*, b^*) of this system can be induced from following equations:

$$\begin{aligned} 0 &= F(a^*)b^* - k_{off}a^*, \\ 0 &= -F(a^*)b^* + k_{off}a^* + g_{on}(N - a^*L - b^*L)Q(a^*, b^*) - g_{off}b^*. \end{aligned}$$

To access the stability of homogeneous steady state with respect to small perturbations, we define $a(x,t)$ and $b(x,t)$ as slightly perturbed functions from the homogeneous steady state:

$$a(x,t) = a^* + \varepsilon a_1(x,t), \tag{A.2a}$$

$$b(x,t) = b^* + \varepsilon b_1(x,t), \tag{A.2b}$$

where the perturbation amplitude $\epsilon \ll 1$ is much smaller than a^* and b^*. After substituting (A.2a) and (A.2b) into the model (1a)–(1b) and applying Taylor expansion at a^* with the first order approximation, $F(a) = F(a^*) + F'(a^*)(a - a^*)$, the leading term satisfies the following system:

$$\frac{\partial a_1}{\partial t} = D_m \nabla^2 a_1 + F(a^*)b_1 + a_1 b^* F'(a^*) - k_{off}a_1, \tag{A.3a}$$

$$\begin{aligned} \frac{\partial b_1}{\partial t} &= D_m \nabla^2 b_1 - F(a^*)b_1 - a_1 b^* F'(a^*) + k_{off}a_1 - g_{on}\frac{(a_1 + b_1)}{\Omega} \\ &\times\ (N - a^*L - b^*L) - g_{on}(\widetilde{a_1} + \widetilde{b_1})Q(a^*, b^*) - g_{off}b_1, \end{aligned} \tag{A.3b}$$

where $F'(a^*)$ denotes the derivative evaluated at a^*. Here we consider a particular spatially periodic perturbation

$$\begin{aligned} a_1(x,t) &= \alpha e^{\lambda(k)t}E_k(x), \\ b_1(x,t) &= \beta e^{\lambda(k)t}E_k(x), \end{aligned}$$

where α and β are non-zero parameters determined by Fourier expansion of the initial conditions in terms of $E_k(x)$, $\lambda(k)$ is the eigenvalue, k is a non-negative integer which represents the wavenumber, and $E_k(x)$ is the kth non-zero eigenfunction of Laplace operator. On the domain $x \in [0, L]$ in a one-dimensional section with periodic boundary, we then have

$$-\nabla^2 E_k(x) = k^2 E_k(x), \quad \text{for} \quad E_k\,|_{x=0} = E_k\,|_{x=L}$$

which is solved by $E_m(x) = a_m \cos(\frac{2m\pi x}{L})$. Here $m = 0, \pm 1, \pm 2, \cdots$ and a_m are constants determined by the initial perturbation. To determine the unstable state, we analyze the stability of the homogeneous steady state points by evaluating the eigenvalues of Jacobian matrix. System (A.3a)–(A.3b) becomes

$$\lambda\begin{pmatrix}\alpha\\ \beta\end{pmatrix}=\begin{pmatrix}-\sigma_m D_m+F'b^*-k_{off} & F\\ -F'b^*+k_{off}-g_{on}\frac{N-a^*L-b^*L}{\Omega}-g_{on}QL\delta(k) & -\sigma_m D_m-F-g_{on}\frac{N-a^*L-b^*L}{\Omega}-g_{on}QL\delta(k)-g_{off}\end{pmatrix}\begin{pmatrix}\alpha\\ \beta\end{pmatrix}, \tag{A.4}$$

where for simplicity, $F(a^*)$ and $F'(a^*)$ are written in F and F'. $\delta(k)$ is a Dirac function, namely, $\delta(k)$ is zero everywhere except at $k=0$ where $\delta(k)=1$ and the eigenvalues

$$\sigma_m=\begin{cases}m^2/R^2 & \text{for a one-dimensional cross section,}\\ 2m^2/R^2 & \text{for a two-dimensional spherical surface,}\end{cases}$$

If we define the Jacobian matrix on the right-hand side of (A.4) as $\mathbf{J}$, then Eq. (A.4) becomes

$$\mathbf{J}\begin{pmatrix}\alpha\\ \beta\end{pmatrix}=\lambda\begin{pmatrix}\alpha\\ \beta\end{pmatrix}. \tag{A.5}$$

Therefore, λ is an eigenvalue of $\mathbf{J}$, and $(\alpha,\beta)^T$ is the corresponding eigenvector. Eq. (A.5) has a nonzero solution (α,β) if and only if $\det(\mathbf{J}-\lambda\mathbf{I})=0$, which means λ should be a root of the following characteristic polynomial:

$$\begin{aligned}&\lambda^2-\lambda\left(-2\sigma_m D_m+F'b^*-F-g_{on}\frac{N-a^*L-b^*L}{\Omega}-g_{on}\delta(k)QL-g_{off}-k_{off}\right)\\&+\sigma_m^2D_m^2+\sigma_m D_m\left(F+g_{on}\frac{N-a^*L-b^*L}{\Omega}+g_{on}\delta(k)QL+g_{off}-F'b^*+k_{off}\right)\\&-(F'b^*-k_{off})\left(g_{on}\frac{N-a^*L-b^*L}{\Omega}+g_{on}\delta(k)QL+g_{off}\right)\\&+F\left(g_{on}\frac{N-a^*L-b^*L}{\Omega}+g_{on}\delta(k)QL\right)=0.\end{aligned} \tag{A.6}$$

Together, these two conditions imply that wave functions perturbed from the homogeneous steady state are moving toward another steady state for and only for positive wavelengths. The first condition is equivalent to that when $k=0$, hence $\sigma_m=0$ and $\delta(k)=1$, the trace of $\mathbf{J}$ is negative and the determinant of $\mathbf{J}$ is positive:

$$F'b^*-F-g_{on}\frac{N-a^*L-b^*L}{\Omega}-g_{on}QL-g_{off}-k_{off}<0, \tag{A.7}$$

and

$$-(F'b^*-k_{off})\left(g_{on}\frac{N-a^*L-b^*L}{\Omega}+g_{on}QL+g_{off}\right)+F\left(g_{on}\frac{N-a^*L-b^*L}{\Omega}+g_{on}QL\right)>0. \tag{A.8}$$

Inequality (A.8) can be rewritten as

$$F'b^*-k_{off}-\frac{g_{on}\frac{N-a^*L-b^*L}{\Omega}+g_{on}QL}{g_{on}\frac{N-a^*L-b^*L}{\Omega}+g_{on}QL+g_{off}}F<0. \tag{A.9}$$

It is easy to show (A.9) implies (A.7), and therefore one only needs to check the inequality (A.9) for condition **(i)**. The second condition is equivalent to the conditions that for some positive k, hence $\delta(k)=0$, the trace of $\mathbf{J}$ is positive or the determinant of $\mathbf{J}$ is negative:

$$-2\sigma_m D_m+F'b^*-F-g_{on}\frac{N-a^*L-b^*L}{\Omega}-g_{off}-k_{off}>0, \tag{A.10}$$

or

$$\begin{aligned}&\sigma_m^2D_m^2+\sigma_m D_m\left(-F'b^*+F+g_{on}\tfrac{N-a^*L-b^*L}{\Omega}+g_{off}+k_{off}\right)\\&-(F'b^*-k_{off})\left(g_{on}\tfrac{N-a^*L-b^*L}{\Omega}+g_{off}\right)+Fg_{on}\tfrac{N-a^*L-b^*L}{\Omega}<0,\quad k\geqslant 1.\end{aligned} \tag{A.11}$$

Inequality (A.11) can be rewritten as

$$-\sigma_m D_m+F'b^*-k_{off}-\frac{\sigma_m D_m+g_{on}\frac{N-a^*L-b^*L}{\Omega}}{\sigma_m D_m+g_{on}\frac{N-a^*L-b^*L}{\Omega}+g_{off}}F>0, \tag{A.12}$$

It can be observed that inequality (A.10) implies (A.12). So it suffices to check the inequality (A.12) for condition **(ii)**. Moreover, if there exists the critical wavenumber k_c such that for any positive integer $k\leqslant k_c$, the second condition can be reduced to the inequality (A.14) below. Finally, we summarize that Turing instability exists at a homogeneous solution (a^*,b^*) if the system (1a)–(1b) satisfies the following two conditions

$$F'b^*-k_{off}-\frac{g_{on}\frac{N-a^*L-b^*L}{\Omega}+g_{on}QL}{g_{on}\frac{N-a^*L-b^*L}{\Omega}+g_{on}QL+g_{off}}F<0, \tag{A.13}$$

and

$$-\sigma_1 D_m+F'b^*-k_{off}-\frac{\sigma_m D_m+g_{on}\frac{N-a^*L-b^*L}{\Omega}}{\sigma_m D_m+g_{on}\frac{N-a^*L-b^*L}{\Omega}+g_{off}}F>0. \tag{A.14}$$

Appendix B. Derivation of power spectrum

Some details of derivation of power spectrum given in Eq. (13) are shown here. The power spectra of stochastic fluctuations in active molecule and inactive molecule correspond to $P_1(k_0,\omega)$ and $P_2(k_0,\omega)$ where just let the species index $r=1$ and $r=2$ in general form of power spectrum formula. According to the definition of power spectrum of stochastic fluctuation, it gives

$$P_r(k_0,\omega)=\langle|\hat{\phi}_r(k_0,\omega)|^2\rangle=\langle\hat{\phi}_r(k_0,\omega)\overline{\hat{\phi}_r(k_0,\omega)}\rangle$$

where $\overline{(\cdot)}$ denotes conjugate. To solve $\hat{\phi}_r(k_0,\omega)$ by (10), we introduce $\Phi_{rl}(k_0,\omega)$ and it yields

$$\hat{\phi}_r(k_0,\omega)=\sum_{l=1}^{2}\Phi_{rl}^{-1}(k_0,\omega)\hat{\mu}_l(k_0,\omega),$$

where $\langle\hat{\mu}_r(\omega)\overline{\hat{\mu}_m(\omega)}\rangle=\hat{M}^*_{rm}$, $\Phi_{rl}(k_0,\omega)=i\omega I_{rl}-\hat{J}_{rl}(k_0,\omega)$ and I_{rl} is 2×2 identity matrix. Since $\hat{\phi}_r=\sum_{l=1}^{2}\Phi_{rl}^{-1}\hat{\mu}_l$ in above equation, here for simplicity (k_0,ω) was omitted, so the power spectrum becomes:

$$\begin{aligned}
P_r(k_0,\omega)&=\sum_{l=1}^{2}\Phi_{rl}^{-1}\hat{\mu}_l\overline{\left(\sum_{m=1}^{2}\Phi_{rm}^{-1}\hat{\mu}_m\right)}\\
&=\sum_{l=1}^{2}\Phi_{rl}^{-1}\hat{\mu}_l\left(\sum_{m=1}^{2}\overline{\hat{\mu}_m}\left(\overline{\Phi}\right)^{-1}_{rm}\right)\\
&=\sum_{l=1}^{2}\sum_{m=1}^{2}\Phi_{rl}^{-1}\hat{\mu}_l\overline{\hat{\mu}_m}\left(\Phi^{-1}\right)^H_{rm}\\
&=\sum_{l=1}^{2}\sum_{m=1}^{2}\Phi_{rl}^{-1}\hat{M}^*_{lm}\left(\Phi^{-1}\right)^H_{rm}.
\end{aligned}$$

where $(\cdot)^H$ is the conjugate transpose. Here Φ is a 2×2 matrix, and the inverse Φ^{-1} and its conjugate transpose $\left(\Phi^{-1}\right)^H$ would be formulated by the components of Φ as following:

$$\begin{aligned}
\Phi^{-1}&=\frac{1}{\Phi_{11}\Phi_{22}-\Phi_{12}\Phi_{21}}\begin{pmatrix}\Phi_{22}&-\Phi_{12}\\-\Phi_{21}&\Phi_{11}\end{pmatrix},\\
\left(\Phi^{-1}\right)^H&=\frac{1}{\overline{\Phi_{11}\Phi_{22}}-\overline{\Phi_{12}\Phi_{21}}}\begin{pmatrix}\overline{\Phi_{22}}&-\overline{\Phi_{12}}\\-\overline{\Phi_{21}}&\overline{\Phi_{11}}\end{pmatrix}
\end{aligned}$$

where

$$\begin{aligned}
\Phi_{11}&=i\omega-\hat{J}^*_{11}, & \Phi_{12}&=-\hat{J}^*_{12},\\
\Phi_{21}&=-\hat{J}^*_{21}, & \Phi_{22}&=i\omega-\hat{J}^*_{22},\\
\overline{\Phi_{11}}&=-i\omega-\hat{J}^*_{11}, & \overline{\Phi_{12}}&=-\hat{J}^*_{12},\\
\overline{\Phi_{21}}&=-\hat{J}^*_{21}, & \overline{\Phi_{22}}&=-i\omega-\hat{J}^*_{22}.
\end{aligned}\tag{B.1}$$

Active molecule corresponds to $r=1$ and its power spectrum $P_1(k_0,\omega)$

$$\begin{aligned}
P_1(k_0,\omega)&=\sum_{l=1}^{2}\sum_{m=1}^{2}\Phi_{1l}^{-1}\hat{M}^*_{lm}\left(\Phi^{-1}\right)^H_{1m}\\
&=\Phi_{11}^{-1}\hat{M}^*_{11}\left(\Phi^{-1}\right)^H_{11}+\Phi_{11}^{-1}\hat{M}^*_{12}\left(\Phi^{-1}\right)^H_{12}+\Phi_{12}^{-1}\hat{M}^*_{21}\left(\Phi^{-1}\right)^H_{11}+\Phi_{12}^{-1}\hat{M}^*_{22}\left(\Phi^{-1}\right)^H_{12}\\
&=\frac{\Phi_{22}\hat{M}^*_{11}\overline{\Phi_{22}}}{(\Phi_{11}\Phi_{22}-\Phi_{12}\Phi_{21})(\overline{\Phi_{11}\Phi_{22}}-\overline{\Phi_{12}\Phi_{21}})}-\frac{\Phi_{22}\hat{M}^*_{12}\Phi_{12}}{(\Phi_{11}\Phi_{22}-\Phi_{12}\Phi_{21})(\overline{\Phi_{11}\Phi_{22}}-\overline{\Phi_{12}\Phi_{21}})}\\
&\quad-\frac{\Phi_{12}\hat{M}^*_{21}\overline{\Phi_{22}}}{(\Phi_{11}\Phi_{22}-\Phi_{12}\Phi_{21})(\overline{\Phi_{11}\Phi_{22}}-\overline{\Phi_{12}\Phi_{21}})}+\frac{\Phi_{12}\hat{M}^*_{22}\Phi_{12}}{(\Phi_{11}\Phi_{22}-\Phi_{12}\Phi_{21})(\overline{\Phi_{11}\Phi_{22}}-\overline{\Phi_{12}\Phi_{21}})}\\
&=\frac{\Phi_{22}\hat{M}^*_{11}\overline{\Phi_{22}}-\Phi_{22}\hat{M}^*_{12}\Phi_{12}-\Phi_{12}\hat{M}^*_{21}\overline{\Phi_{22}}+\Phi_{12}\hat{M}^*_{22}\Phi_{12}}{(\Phi_{11}\Phi_{22}-\Phi_{12}\Phi_{21})(\overline{\Phi_{11}\Phi_{22}}-\overline{\Phi_{12}\Phi_{21}})}.
\end{aligned}$$

Substitute the value in (B.1) into the above equation, the power spectrum of active molecule can be written explicitly:

$$P_1(k_0,\omega)=\frac{\hat{M}^*_{11}(\hat{J}^*_{22})^2+\hat{M}^*_{22}(\hat{J}^*_{12})^2-2\hat{M}^*_{12}\hat{J}^*_{12}\hat{J}^*_{22}+\hat{M}^*_{11}\omega^2}{[\omega^2-(\hat{J}^*_{11}\hat{J}^*_{22}-\hat{J}^*_{12}\hat{J}^*_{21})]^2+(\hat{J}^*_{11}+\hat{J}^*_{22})^2\omega^2}.$$

Analogously, we can easily derive the expression for inactive molecule in Eq. (13) with the same manner.

Appendix C. Stochastic Simulation Algorithm

The chemical master Eq. (6) provides exact description of the stochastic process. It can be accessed numerically by SSA. Instead of focusing on concentration of molecules at local area, SSA is based on the number of molecules in discrete space. Consider $\vec{X}(t)$ as a variable with respect to x, the probability that a reaction R or a jump J will happen in the next time interval $[t, t+dt)$ is $\alpha(t)dt$ where α is the propensity function corresponding to the reaction or the jump at time t. In SSA, two random numbers r_1 and r_2, that are uniformly distributed in [0,1], are generated for determining time and index of next reaction, respectively. The time for next reaction is $t+\tau$, with

$$\tau = -\frac{\ln r_1}{\alpha_0(t)},$$

where $\alpha_0(t)$ is the sum of all propensity functions:

$$\alpha_0(t) = \sum_{k=1}^{K}\left(\sum_{j=1}^{4}\alpha_{kj}(t) + \alpha_{LA_k}(t) + \alpha_{RA_k}(t) + \alpha_{LB_k}(t) + \alpha_{RB_k}(t)\right).$$

The index of the next reaction is obtained by finding the smallest m and q such that

$$\sum_{k=1}^{q-1}\sum_{j=1}^{4}\alpha_{kj} + \sum_{j=1}^{m}\alpha_{qj} \geqslant r_2\alpha_0 \tag{C.1}$$

$$\text{or} \quad \sum_{k=1}^{K}\sum_{j=1}^{4}\alpha_{kj} + \sum_{k=1}^{q}\alpha_{LA_k} \geqslant r_2\alpha_0 \tag{C.2}$$

$$\text{or} \quad \sum_{k=1}^{K}\left(\sum_{j=1}^{4}\alpha_{kj} + \alpha_{LA_k}\right) + \sum_{k=1}^{q}\alpha_{RA_k} \geqslant r_2\alpha_0 \tag{C.3}$$

$$\text{or} \quad \sum_{k=1}^{K}\left(\sum_{j=1}^{4}\alpha_{kj} + \alpha_{LA_k} + \alpha_{RA_k}\right) + \sum_{k=1}^{q}\alpha_{LB_k} \geqslant r_2\alpha_0 \tag{C.4}$$

$$\text{or} \quad \sum_{k=1}^{K}\left(\sum_{j=1}^{4}\alpha_{kj} + \alpha_{LA_k} + \alpha_{RA_k} + \alpha_{LB_k}\right) + \sum_{k=1}^{q}\alpha_{RB_k} \geqslant r_2\alpha_0. \tag{C.5}$$

If the condition (C.1) is satisfied, then reaction R_{qm} happens and the state of system is updated as $\vec{X}(t+\tau) = \vec{X}(t) + \nu_{qm}$; or if the condition (C.2) is satisfied, then diffusion jump J_{LA_q} happens and the state of system is updated as $\vec{X}(t+\tau) = \vec{X}(t) + \nu_{LA_q}$; or the condition (C.3) is satisfied, then diffusion jump J_{RA_q} happens and state of the system is updated as $\vec{X}(t+\tau) = \vec{X}(t) + \nu_{RA_q}$; or if the condition (C.4) is satisfied, then diffusion jump J_{LB_q} happens and the state of system is updated as $\vec{X}(t+\tau) = \vec{X}(t) + \nu_{LB_q}$; or the condition (C.5) is satisfied, then diffusion jump J_{RB_q} happens and the state of system is updated as $\vec{X}(t+\tau) = \vec{X}(t) + \nu_{RB_q}$.

Appendix D. Linear feedback loop

Here the linear positive feedback form means that the local positive feedback function (2) has no cooperativity: $F(a) = k_{11} + k_{12}a$. Next we will show this kind feedback form is unable to provide spontaneous onset of cell polarization based on the linear stability analysis we have studied above. With the linear feedback function, we obtain the following

$$0 = (k_{11} + k_{12}a^*)b^* - k_{off}a^*,$$

We can obtain that

$$k_{12}b^* - k_{off} = -k_{11}\frac{b^*}{a^*}.$$

Since the parameter k_{11} and the steady state solution a^*, b^* are positive, the left-hand term $k_{12}b^* - k_{off}$ is obviously negative. Considering the condition (5) with linear feedback function,

$$-\sigma_1 D_m + k_{12}b^* - k_{off} - \frac{\sigma_1 D_m + g_{on}\frac{N-a^*L-b^*L}{\Omega}}{\sigma_1 D_m + g_{on}\frac{N-a^*L-b^*L}{\Omega} + g_{off}}F > 0.$$

This necessary condition for symmetry breaking can not be satisfied with the induced conclusion that $k_{12}b^* - k_{off} < 0$. Therefore, linear positive feedback will be insufficient to lead to spontaneous cell polarization.

Stochastic method by performing SSA with weak feedback strength, (a): $k_{12} = 0.987\,\text{min}^{-1}$ and (b): $k_{12} = 10\,\text{min}^{-1}$, is insufficient to establish localization. Nevertheless, with much larger feedback strength, (c): $k_{12} = 40\,\text{min}^{-1}$ and (d): $k_{12} = 100\,\text{min}^{-1}$, signaling molecules display a clear localization profile.

References

[1] Bryant DM, Mostov KE. From cells to organs: building polarized tissue. Nat Rev Mol Cell Biol 2008;9(11):887–901.
[2] Goryachev AB, Pokhilko AV. Dynamics of Cdc42 network embodies a Turing–type mechanism of yeast cell polarity. FEBS Lett 2008;582(10):1437–43.
[3] Kozubowski L, Saito K, Johnson JM, Howell AS, Zyla TR, Lew DJ. Symmetry-breaking polarization driven by a Cdc42p GEF-PAK complex. Curr Biol 2008;18(22):1719–26.
[4] Howell AS, Savage NS, Johnson SA, Bose I, Wagner AW, Zyla TR, et al. Singularity in polarization: rewiring yeast cells to make two buds. Cell 2009;139(4):731–43.
[5] Howell AS, Jin M, Wu C-F, Zyla TR, Elston TC, Lew DJ. Negative feedback enhances robustness in the yeast polarity establishment circuit. Cell 2012;149(2):322–33.
[6] Liu Y, Lo W-C. Analysis of spontaneous emergence of cell polarity with delayed negative feedback. Math Biosci Eng 2019;16(3):1392–413.
[7] Park H-O, Bi E. Central roles of small GTPases in the development of cell polarity in yeast and beyond. Microbiol Mol Biol Rev 2007;71(1):48–96.
[8] Slaughter B, Smith S, Li R. Symmetry breaking in the life cycle of the budding yeast. Cold Spring Harb Perspect Biol 2009;1(3):a003384.
[9] Altschuler SJ, Angenent SB, Wang Y, Wu LF. On the spontaneous emergence of cell polarity. Nature 2008;454(7206):886–9.
[10] Mori Y, Jilkine A, Edelstein-Keshet L. Wave-pinning and cell polarity from a bistable reaction-diffusion system. Biophys J 2008;94(9):3684–97.
[11] Rätz A, Röger M. Symmetry breaking in a bulk-surface reaction-diffusion model for signalling networks. Nonlinearity 2014;27(8):1805–27.
[12] Sarfaraz W, Madzvamuse A. Classification of parameter spaces for a reaction-diffusion model on stationary domains. Chaos Solitons Fractals 2017;103:33–51.
[13] Pablo M, Ramirez SA, Elston TC. Particle-based simulations of polarity establishment reveal stochastic promotion of Turing pattern formation. PLoS Comput Biol 2018;14(3):1–25.
[14] Cusseddu D, Edelstein-Keshet L, Mackenzie J, Portet S, Madzvamuse A. A coupled bulk-surface model for cell polarisation. J Theor Biol 2019;481:119–35.
[15] Turing AM. The chemical basis of morphogenesis. Bull Math Biol 1990;52(1):153–97.
[16] Jilkine A, Angenent SB, Wu LF, Altschuler SJ. A density-dependent switch drives stochastic clustering and polarization of signaling molecules. PLoS Comput Biol 2011;7(11):1–11.
[17] Walther GR, Marée AFM, Edelstein-Keshet L, Grieneisen VA. Deterministic versus stochastic cell polarisation through wave-pinning. Bull Math Biol 2012;74(11):2570–99.
[18] Lo W-C, Lee ME, Narayan M, Chou C-S, Park H-O. Polarization of diploid daughter cells directed by spatial cues and GTP hydrolysis of Cdc42 in budding yeast. PLoS One 2013;8(2):1–14.
[19] Ozbudak EMBecskei A, van Oudenaarden A. A system of counteracting feedback loops regulates Cdc42p activity during spontaneous cell polarization. Dev Cell 2005;9(4):565–71.
[20] Meinhardt H. Models of biological pattern formation. Academic Press; 1982.
[21] Lo W-C, Park H-O, Chou C-S. Mathematical analysis of spontaneous emergence of cell polarity. Bull Math Biol 2014;76(8):1835–65.
[22] Van Kampen NG. Stochastic process in physics and chemistry, vol 1. Amsterdam: Elsevier Science; 1992.
[23] McKane AJ, Nagy JD, Newman TJ, Stefanini MO. Amplified biochemical oscillations in cellular systems. J Stat Phys 2007;128(1):165–91.
[24] Cantini L, Cianci C, Fanelli D, Massi E, Barletti L. Linear noise approximation for stochastic oscillations of intracellular calcium. J Theor Biol 2014;349:92–9.
[25] Risken H. Fokker-Planck equation. Berlin, Heidelberg: Springer Berlin Heidelberg; 1984. ISBN 978-3-642-96807-5
[26] Owolabi KM. High-dimensional spatial patterns in fractional reaction-diffusion system arising in biology. Chaos Solitons Fractals 2020;134:109723.
[27] Lugo CA, McKane AJ. Quasicycles in a spatial predator-prey model. Phys Rev E 2008;78:051911.
[28] Ziman MPreuss D, Mulholland J, O'brien JM, Botstein D, Johnson DI. Subcellular localization of Cdc42p, a Saccharomyces cerevisiae GTP-binding protein involved in the control of cell polarity.. Mol Biol Cell 1993;4(12):1307–16.
[29] Lawson MJ, Drawert B, Khammash M, Petzold L, Yi T-M. Spatial stochastic dynamics enable robust cell polarization. PLoS Comput Biol 2013;9(7):1–12.
[30] Biancalani T, Galla T, J McKane A. Stochastic waves in a Brusselator model with nonlocal interaction. Phys Rev E 2011;84:026201.
[31] Trogdon M, Drawert B, Gomez C, Banavar SP, Yi T-M, Camps O, et al. The effect of cell geometry on polarization in budding yeast. PLoS Comput Biol 2018;14(6):1–22.